ADVANCED HEALTHCARE MATERIALS
www.advhealthmat.de

Reconfigurable Hanging Drop Microarray Platform for On-Demand Preparation and Analysis of Spheroid Array

*Hwisoo Kim, Bumsoo Kim, Soo Jee Kim, Yejin Choi, Irene Hae-Rim Kim, Jieun Han, Young-Gyun Park, Yong-Mahn Han, and Je-Kyun Park**

In response to the increasing demand for spheroid-based cancer research, the importance of developing integrated platforms that can simultaneously facilitate high-throughput spheroid production and multiplexed analysis is emphasized. In addition, the understanding of how the size and cellular composition of tumors directly influence their internal structures and functionalities underlines the critical need to produce spheroids of diverse sizes and compositions on a large scale. To address this rising demand, this work presents a configurable and linkable in vitro three-dimensional (3D) cell culture kit (CLiCK) for spheroids, termed CLiCK-Spheroid. This platform consists of three primary components: a hanging drop microarray (HDMA), a concave pillar microarray (CPMA), and gradient blocks. The HDMA alone produces a homogeneous spheroid array, while its combination with the gradient block enables one-step generation of a size-gradient spheroid array. Using the size-gradient spheroid arrays, the occurrence of necrotic cores based on spheroid size is demonstrated. Additionally, spheroids in a single batch can be conveniently compartmentalized and regrouped using a CPMA, enhancing the versatility of spheroid arrays and enabling multiplexed drug treatments. By combining the different assembly methods, this work has achieved high-throughput production of cell composition-gradient spheroid arrays, with noticeable variations in morphology and vascularization based on cell compositions.

1. Introduction

In vitro cell culture and in vivo animal models have consistently been employed to research disease mechanisms and drug screening. However, with the growing emphasis on animal welfare and bioethics, the trend is gradually shifting toward reducing animal experiments.[1–3] Instead, there is an increased interest in in vitro three-dimensional (3D) cell culture models due to their increased fidelity, owing to the heightened relevance of the models and the introduction of induced pluripotent stem cells and patient-derived cells.[4–7] In particular, spheroids are an effective 3D cell culture model as they are relatively easy to produce and can recapitulate structural and functional features of in vivo microenvironments.[8–10] While methods to produce spheroids have advanced significantly, high-throughput screening requires spheroids to exist in a separate array environment. Hanging drop and low-adhesion well plates are prominent examples of the separate array environment. These systems allow for the precise control of cell type, cell number, and reagent change of multiple conditions, but the cell seeding and reagent change procedures are labor-intensive and difficult to parallelize without the assistance of a machine.[11] In addition, hanging drop plates are also susceptible to evaporation. Consequently, various methods, such as microwell array platforms, have been developed to generate large-scale spheroid arrays at once.[12,13] Another study demonstrated the large-scale production of spheroids using a funnel

H. Kim, S. J. Kim, Y. Choi, I. H.-R. Kim, J. Han, Y.-G. Park, J.-K. Park
Department of Bio and Brain Engineering
Korea Advanced Institute of Science and Technology (KAIST)
291 Daehak-ro, Yuseong-gu, Daejeon 34141, Republic of Korea
E-mail: jekyun@kaist.ac.kr

The ORCID identification number(s) for the author(s) of this article can be found under https://doi.org/10.1002/adhm.202400501

DOI: 10.1002/adhm.202400501

B. Kim
Department of Biological Sciences
Korea Advanced Institute of Science and Technology (KAIST)
291 Daehak-ro, Yuseong-gu, Daejeon 34141, Republic of Korea

Y.-M. Han
Graduate School of Medical Science and Engineering
Korea Advanced Institute of Science and Technology (KAIST)
291 Daehak-ro, Yuseong-gu, Daejeon 34141, Republic of Korea

J.-K. Park
KI for Health Science and Technology
KAIST Institutes (KI)
291 Daehak-ro, Yuseong-gu, Daejeon 34141, Republic of Korea

J.-K. Park
KI for NanoCentury
KAIST Institutes (KI)
291 Daehak-ro, Yuseong-gu, Daejeon 34141, Republic of Korea

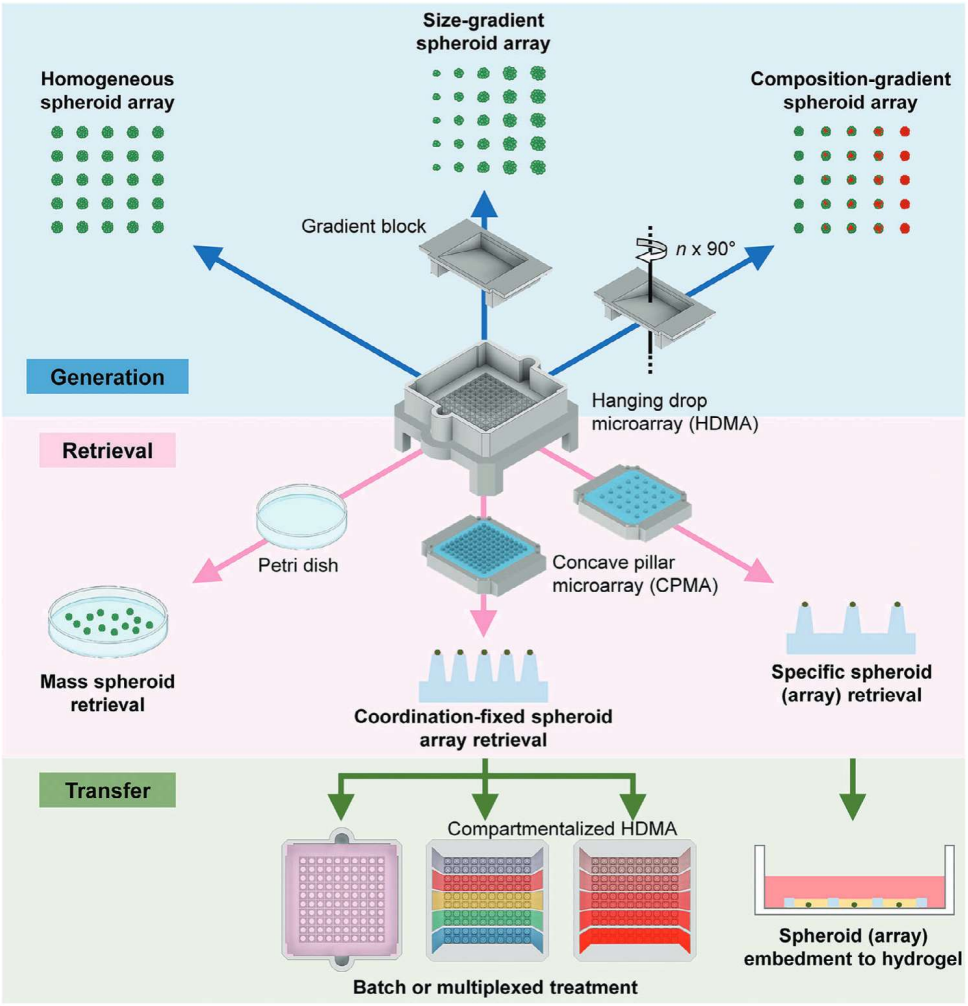

Figure 1. Schematic illustrations of the components and functions of a configurable and linkable in vitro 3D cell culture kit for spheroids (CLiCK-Spheroid). The hanging drop microarray (HDMA) facilitates the generation of a homogeneous spheroid array, which can be collected on a Petri dish. By applying a gradient block to the HDMA, a size-gradient spheroid array and a composition-gradient spheroid array can be generated. The generated spheroid array can be retrieved entirely or selectively by contacting the concave pillar microarray (CPMA), while retaining their spatial arrangement. Thus, the spheroid array can be transferred freely from batch to compartmentalized environment and vice versa.

array to simultaneously generate hanging drop arrays.[14] While these methods successfully generate homogeneous spheroids at a large scale, their applicability to high-throughput screening is limited due to their interconnected environment, which prevents the creation of compartmentalized and multiplexed cell culture and analysis.

Meanwhile, the size and composition of spheroids play crucial roles in determining their function, viability, and response to drugs.[15,16] Studies have shown that as the spheroid size increases, a hypoxic region and necrotic core can form within the spheroid.[17] These factors can significantly influence various aspects of spheroid behavior, including extracellular matrix remodeling,[18] metastasis,[19] and drug resistance. Additionally, co-culture and tri-culture spheroids composed of multiple cell types have gained considerable attention as they can better mimic the tumor microenvironment and provide a more realistic model for studying disease progression and therapeutic interventions.[20] However, the generation of large-scale and heterogeneous spheroid arrays remains a challenge. Current approaches, primarily based on microwell plates, are often labor-intensive and time-consuming. These methods fail to efficiently generate arrays of diverse spheroid compositions and sizes, limiting their applicability in studying complex biological phenomena and drug screening. To address the problem of labor-intensiveness, Marimuthu et al. demonstrated the formation of a size-gradient spheroid array using multi-sized microfluidic funnels[21] and other studies showed an area-based size-gradient spheroid array formation.[22–24] While these studies effectively exhibited the fabrication of single ratio size-gradient spheroid arrays, there remains a pressing need to develop novel high-throughput techniques that enable the production of large-scale cell composition-gradient spheroid arrays in a more efficient and reproducible manner.

In this study, we introduce a configurable and linkable in vitro 3D cell culture kit (CLiCK) for spheroid, termed CLiCK-Spheroid, which is a novel hanging drop microarray platform designed specifically for on-demand generation and multiplexed analysis of spheroid arrays (**Figure 1**). CLiCK-Spheroid comprises three

main components: hanging drop microarray (HDMA), concave pillar microarray (CPMA), and gradient block. The proposed kit enables researchers to easily prepare spheroid arrays according to their specific requirements, including homogeneous arrays, size-gradient arrays, and cell composition-gradient arrays. Furthermore, CLiCK-Spheroid provides a convenient method for separating spheroids into discrete environments, allowing for individualized analysis and experimentation. Additionally, this platform facilitates the efficient retrieval and transfer of the entire and localized spheroid array for downstream applications. With its user-friendly design and enhanced functionality, CLiCK-Spheroid is expected to become a valuable tool for biologists to open new possibilities for advancing various research areas, including tumor biology, personalized medicine, and drug discovery.

2. Results

2.1. One-Step Generation of a Homogeneous Spheroid Array

An HDMA is conceptualized and fabricated to generate a spheroid array in a hanging drop form (**Figure** 2a,b). The bottom part of the HDMA features a funnel-shaped hole array in which cell suspension, media, and reagents can be loaded through pipetting from the loading ports. All the holes are connected from the top to a reservoir with a maximum volume of 1.6 mL. When cell suspension is loaded in the HDMA, the seeded cells are distributed and settled into each hole. By removing the supernatants and adding media to the HDMA, the homogeneous spheroid array could be formed in the HDMA at once (Figure S1a, Supporting Information). The size of the spheroid exhibited a correlation with the cell concentration, the area of the upper part of the funnel, and the average height of the liquid above the funnel, as depicted in Figure 2c. When BT474 cells, one of breast cancer cell line, were seeded into the HDMA, the cells formed spheroids within 24 h (Figure 2d,e).

In order to assess the homogeneity of the spheroid array formed in the HDMA, we seeded 500 000 BT474 cells into HDMAs with different hole sizes and array dimensions (Figure S2a, Supporting Information). Arrays of different dimensions were designed while keeping the overall size of the array constant, thus leading to different hole sizes. The results demonstrated the generation of homogeneous spheroid arrays, with the size of the spheroids being proportional to the hole size (Figure S2b, Supporting Information). Specifically, the diameters of the spheroids in the 10 × 10 (1.5 mm square top and 1 mm circular bottom), 12 × 12 (1.25 mm square top and 0.833 mm circular bottom), and 15 × 15 (1 mm square top and 0.667 mm circular bottom) HDMAs were 370.3 ± 22.5, 332 ± 17.4, and 282 ± 13.3 μm, respectively. The coefficient of variance (CV) for each HDMA was 6.09%, 5.23%, and 4.71%, indicating a high level of spheroid homogeneity across all the HDMAs. This level of uniformity is significantly higher than that reported by Sumi et al. (34.97%, 16.85%, and 23.33%).[14] This enhanced uniformity is likely due to differences in device design. The histogram depicted in Figure 2f also showed that the spheroids generated in the HDMAs were monodispersed (CV = 6.09%). To investigate whether the position of the spheroid in the array affects its diameter, we analyzed the average spheroid diameter at each position (Figure 2g). As a result, we confirmed that spheroids of highly homogeneous sizes were generated in the HDMAs, although slightly larger spheroids were found along the edges of the array. To find out the relationship between seeded cell numbers and the actual number of cells settled into each hole, we derived an empirical equation showing the relationship between the spheroid diameter and the number of seeded cells. We seeded green fluorescent protein (GFP)-BT474 cells in each well of a conventional ultra-low attachment 96-well plate, starting with 50 cells and doubling the number up to 6400 cells. We have determined that the relationship between BT474 spheroid diameter on day 1 and the number of BT474 cells within the investigated range follows Equation (1) below:

$$\text{Number of seeded cells} = \left(\frac{\text{Diameter of spheroid at day 1}}{16.83865}\right)^{2.66638} \quad (1)$$

As Equation (1) was derived empirically, it should be noted that its application is limited to BT474 spheroids on day 1. From this equation, we calculated the number of cells settled in each hole (Figure 2h). The average number of settled cells in 10 × 10 HDMA was 3760 in each hole. This corresponds to ≈376 000 cells settled in the whole array, which was 75.2% of the initially seeded cells. Considering that the holes occupy 58.22% of the total surface area of the HDMA bottom, theoretically, there should be 2910 cells present in each hole. In practice, the presence of flow during pipetting and the influx of cells from the bottom surface of the reservoir bordering the holes can contribute to the observed increase in the number of cells settled in the holes. Consistent with this finding, when seeding 100 000 cells, spheroids with an average diameter of ≈203.1 ± 5.8 μm were generated (CV = 2.86%). According to the previous empirical equation, this corresponds to a spheroid composed of ≈760 cells. Therefore, it can be inferred that in the current design of the 10 × 10 HDMA, ≈0.76% of the total seeded cells are settled into each hole.

During medium or reagent changes in the HDMA, there was a risk of loss and unintended movement of spheroids. To prevent this, a mesh insert is designed to fit the reservoir of the HDMA (Figure S3a, Supporting Information). The mesh was sterilized in ethanol, washed twice with phosphate-buffered saline (PBS), and then immersed in an anti-cell adherence solution before placement into the HDMA with the spheroid array. In the absence of the mesh insert, movement of spheroids near the pipette tip to other holes during medium changes was observed (Figure S3b, Video S1, Supporting Information). However, with the mesh insert in place, the spheroid arrays were successfully retained at their initial positions (Figure S3c, Video S2, Supporting Information). In comparison to the results of reagent change with gentle pipetting, the spheroid retention rate was higher when using the mesh insert, despite harsh pipetting (Figure S3d, Supporting Information). Therefore, the mesh insert was used during the reagent change process to maintain the spheroids in their original position.

Next, we monitored the growth of spheroids over time to investigate the maintenance of spheroid array homogeneity. By examining the spheroid images, it was evident that the spheroids increased in size over 7 days of observation (Figure S4a, Supporting Information). Similar growth patterns were observed when comparing the spheroids seeded with 500 000 cells (3760 cells per hole) in the 10 × 10 HDMAs and the spheroids seeded with 3200

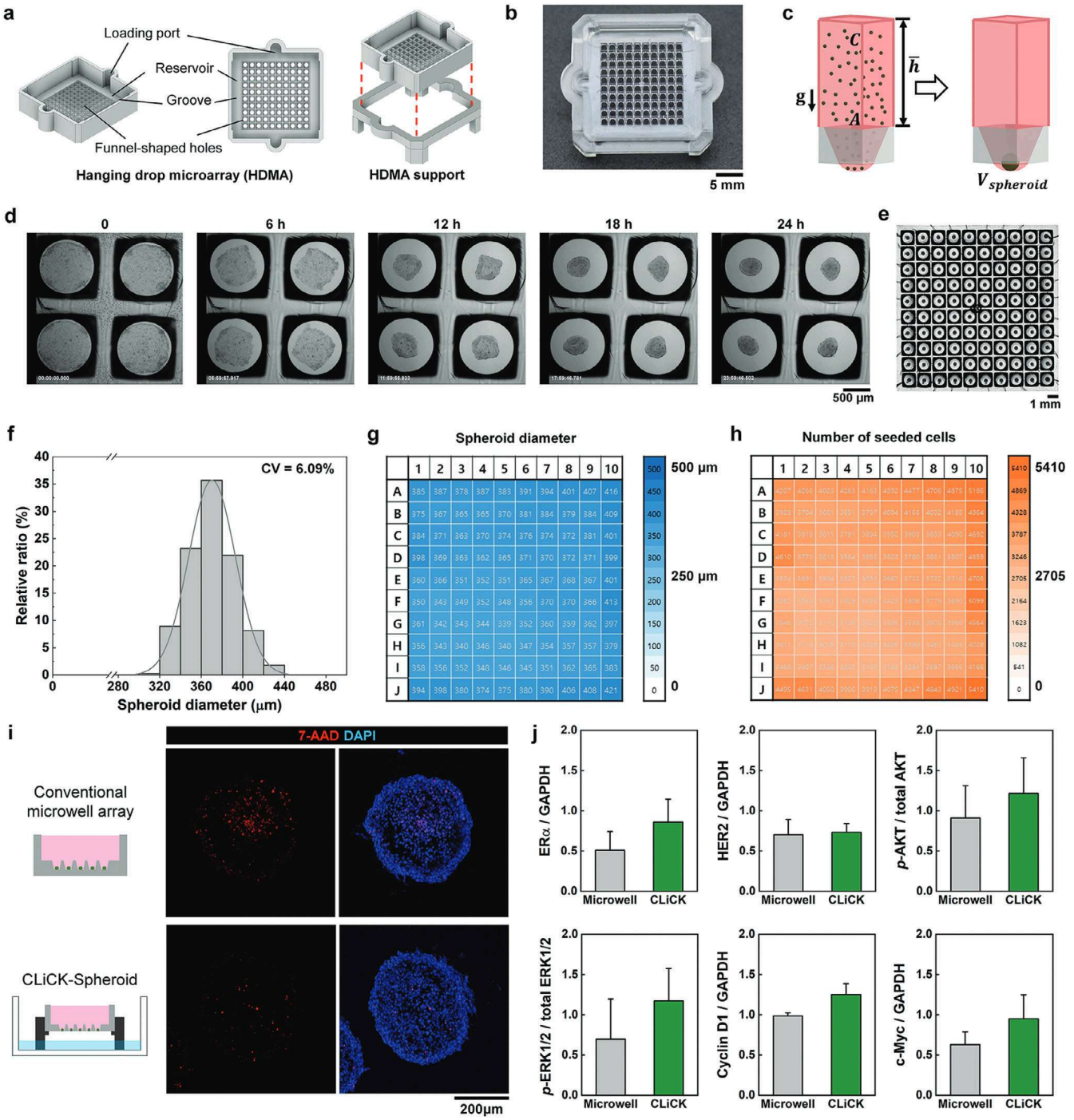

Figure 2. Device configuration and operation procedures of CLiCK-Spheroid for generating a homogeneous spheroid array. a) Design of HDMA, HDMA support, and assembly method. b) A picture of the HDMA assembled with HDMA support. c) Theoretical principle of spheroid formation. The gray structure indicates one funnel of HDMA. The volume (***V***) of the spheroid is proportional to the area of the top of the funnel (***A***), the average height of the liquid above the funnel ($\bar{h}$), and the concentration of the cell suspension (***C***). d) Microscope images of the BT474 spheroid formation in the first 24 h. e) The produced BT474 spheroid array in the 10 × 10 HDMA. f) Histogram of the spheroid diameter in the 10 × 10 HDMAs ($n = 400$ spheroids). g,h) Heatmaps of g) spheroid diameter and h) number of seeded cells in the 10 × 10 HDMAs ($n = 400$ spheroids). i) Fluorescence images of spheroid sections generated using the conventional microwell arrays and CLiCK-Spheroid. Red fluorescence indicates dead cells stained with 7-aminoactinomydin D (7-AAD), and blue fluorescence indicates nuclei stained with 4′,6-diamidino-2-phenylindole (DAPI). j) Western blotting results of expression of markers for comparing day 7 BT474 spheroids from the conventional microwell array and CLiCK-Spheroid. Graphs showing the expression of breast cancer receptors, AKT signaling pathway, MAPK signaling pathway, and cell proliferation ($n = 3$).

cells per well in the conventional ultra-low attachment well plate (Figure S4b, Supporting Information). The CV of the spheroid diameter in the HDMA was 6.09% on day 1, 5.33% on day 3, and 5.46% on day 7, indicating that the homogeneity of the spheroid array in the HDMA was well maintained over time. Spheroid growth was analyzed position-by-position to investigate the potential differences in spheroid growth based on their positions within the array (Figure S4c, Supporting Information). Using the spheroid sizes on day 1 as a reference, we compared the spheroid sizes on days 3 and 7 to determine the relative growth rate of the spheroids. Spheroid growth was slightly more pronounced toward the edges of the array than the center over time. This disparity can be resolved by increasing the frequency of medium changes to prevent nutrient depletion or increasing the volume of medium replaced during each medium change process. However, this trend did not significantly affect the overall homogeneity of the spheroid array, as the CVs on day 1, day 3, and day 7 were similar.

When comparing day 7 spheroids of similar size from CLiCK-Spheroid and the conventional microwell array, we found that the spheroid from the microwell array showed more dead cells than that from CLiCK-Spheroid (Figure 2i and Figure S5a, Supporting Information). Furthermore, we confirmed protein expression by western blot analysis to determine whether the difference exists between the spheroids from the conventional microwell array and CLiCK-Spheroid (Figure 2j and Figure S5b, Supporting Information). As a result, an increase in the marker expressions for breast cancer receptors (estrogen receptor (ER) and human epidermal growth factor receptor 2 (HER2)), the AKT signaling pathway, the mitogen-activated protein kinase (MAPK) signaling pathway, and cell proliferation markers (c-Myc and Cyclin D1) were observed in CLiCK-Spheroid, but the differences were statistically insignificant. From these results, we were able to confirm that our system is just as effective or even better than conventional methods in maintaining the identity of cancer cells and promoting cell proliferation.

2.2. One-Step Generation of a Size-Gradient Spheroid Array

To generate size-gradient spheroid arrays in the HDMA rather than homogeneous arrays, a gradient block was introduced (**Figure 3a**). The gradient block consists of two main structures: a gradient-generating slope and aligning parts. The aligning parts of the gradient blocks were designed to fit into the grooves of the HDMA, enabling reversible assembly. When the gradient block was assembled with the HDMA, the height above each hole varied along the gradient-generating slope. As a result, when the cell suspension was loaded into the HDMA with the gradient block, different numbers of cells settled into each hole (Figure S1b, Supporting Information). As depicted in Figure 3b, no leakage was observed when the cell suspension was loaded into the gradient block-assembled HDMA. Through microscopic imaging, a successful formation of the size-gradient spheroid array was observed along the slope of the gradient block. An increase along the gradient slope was observed in the analysis of the spheroid diameter by column (Figure 3c). However, we found that as the column number increases, the change in diameter becomes less significant. This is due to the linear nature of the gradient-generating slope. In theory, a linear slope results in a proportional distribution of cells. This means that the volume of the generated spheroids has a proportional relationship, and consequently, the diameter follows a curve of 1/3 power, leading to a reduction in differences at higher column numbers. The number of seeded cells per position calculated using Equation (1) shows a linear increase based on the column (Figure 3d). The relationship can be described by the following equation:

$$\text{Number of seeded cells in each position} = 574.515 \times \text{column number} - 534.644 \quad (2)$$

Equation (2) demonstrated a high coefficient of determination (R^2 value of 99.2%), indicating that the number of seeded cells was effectively controlled using the gradient block.

To assess the difference in spheroid zonation within the size-gradient spheroid array generated using CLiCK-Spheroid, live/dead staining was performed. BT474 cells were seeded at a concentration of 500 000 cells per device to assess the occurrence of a necrotic core. In our experiments, among the BT474 spheroids generated in an HDMA, only the spheroids in columns 5 to 10 exhibited necrotic cores (Figure 3e). The size of the necrotic core was proportional to the spheroid size (Figure 3f). When the seeding concentration was set to 250 000 cells per device, the occurrence of the necrotic core was observed in spheroids with diameters exceeding 540 µm (Figure S6a, Supporting Information). Our findings reveal that necrotic cores were observed starting from larger spheroids of 540 µm in size, which aligns with existing research indicating that necrotic cores typically appear in spheroids larger than 500 µm,[25] but with a slightly larger threshold value. This phenomenon may be attributed to the oxygen-rich environment of the hanging drop, as also observed in Figure 2i. On the other hand, when the size-gradient spheroid array was generated by mixing lung fibroblasts (LF) and human umbilical vein endothelial cells (HUVEC) with BT474 cells at a ratio of BT474: LF: HUVEC = 3:1:1, with a total seeding concentration of 250 000 cells per device, the occurrence of the necrotic core was observed even in spheroids with a diameter below 500 µm (Figure S6b, Supporting Information). Necrotic cores appeared in spheroids with diameters above 350 µm, and when compared to BT474 mono-type spheroids under the same conditions, larger necrotic cores were observed. This indicates that spheroids of the same size may differ in compactness depending on the cell type due to the variation in cell-to-cell interaction forces. Considering the studies reported that fibroblasts are often found in the core of co-culture spheroids,[26–28] it can be inferred that the LF region in the core was more compact than the BT474 region, and it leads to the easy occurrence of hypoxic and necrotic core. In conclusion, it is not feasible to establish a general threshold size for necrotic core occurrence, as it can vary depending on the type of cells involved or the culture method applied.

2.3. Multiplexed Drug Condition Treatment in a Single Spheroid Array

For stable retrieval and multiplexed condition treatment of the generated spheroid array, a concave pillar microarray (CPMA)

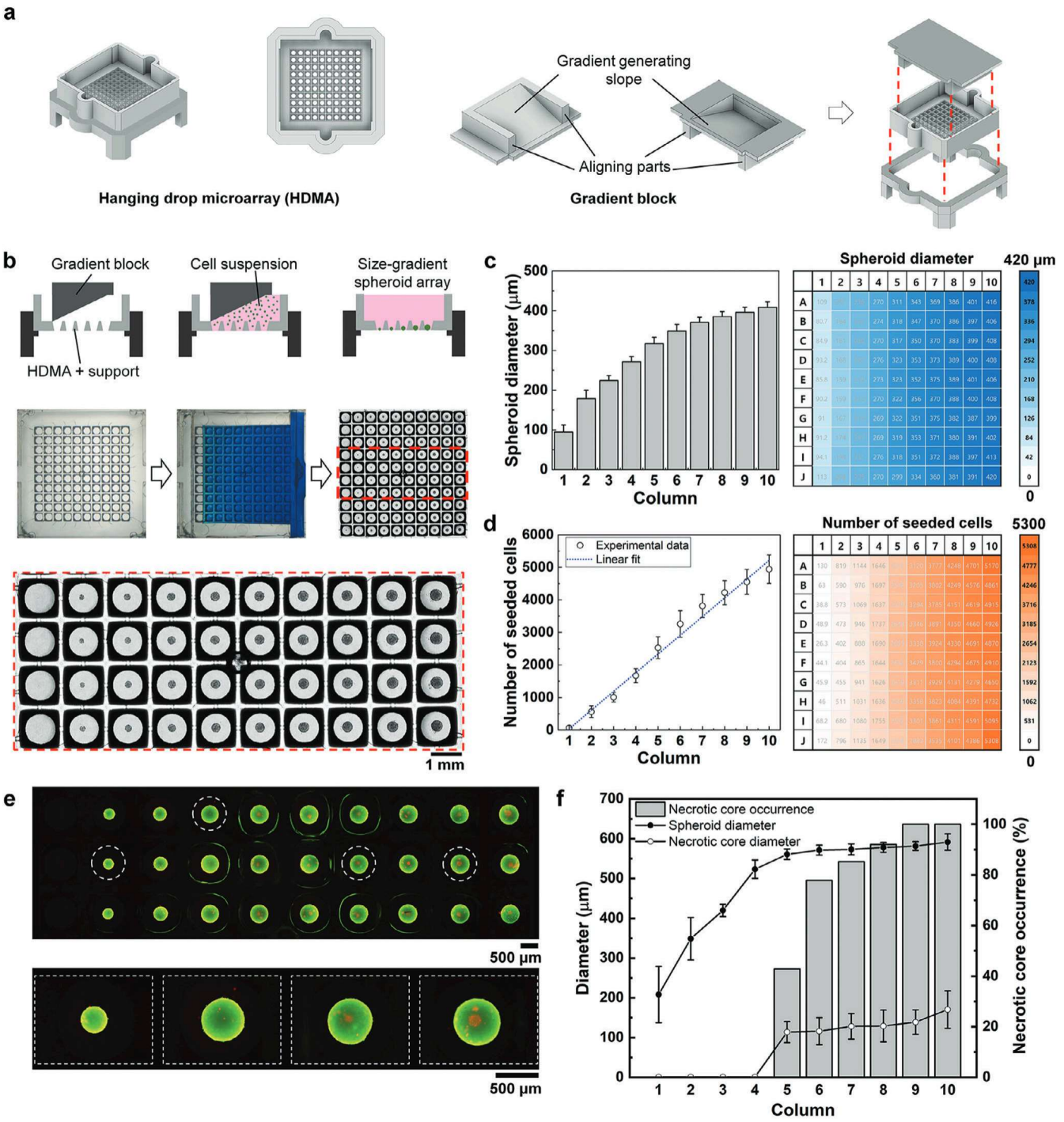

Figure 3. CLiCK-Spheroid for generating a size-gradient spheroid array. a) Configuration and assembly method of CLiCK-Spheroid for generating a size-gradient spheroid array. The aligning parts of the gradient blocks are designed to fit into the grooves of the HDMAs. b) Schematic diagrams and real images illustrating the generation of size-gradient spheroid arrays using CLiCK-Spheroid (top). The size-gradient spheroid arrays were obtained on day 1, with an initial seeding number of 375 000 cells (bottom). c,d) Graphs and heatmaps showing c) spheroid diameter and d) number of seeded cells at each position in the array. e) Fluorescence images showing the day 7 BT474 spheroid array stained with calcein-AM (green) and propidium iodide (red). The initial seeding concentration was 500 000 cells per device. Yellow dotted circles indicate the locations of spheroids used for magnified images. f) A graph of the diameters of spheroids and necrotic cores, and the ratio of necrotic core occurrence according to the column number ($n = 3$).

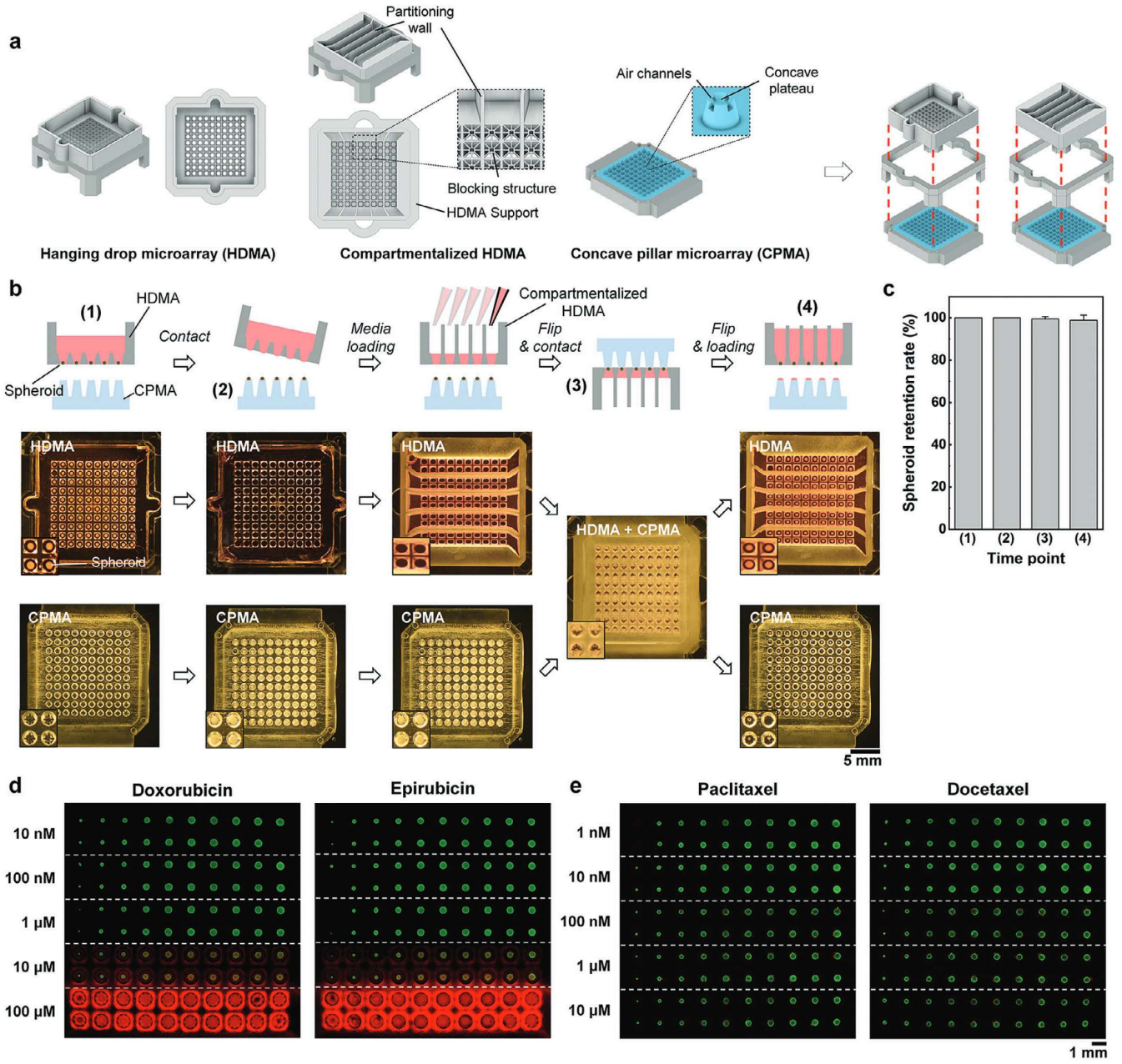

Figure 4. Multiplexed drug treatment and assays in a single spheroid array. a) Configuration and assembly method of CLiCK-Spheroid for retrieval and compartmentalization of spheroid arrays. The edges of the CPMA are designed to fit inside the legs of the HDMA support, enabling easy alignment by the naked eye. b) Schematic illustrations (top) and real images (bottom) of operational procedures for spheroid array retrieval and compartmentalization. The numbers in parentheses indicate the corresponding time points. c) Graph depicting the spheroid retention rate at the time point indicated in panel b ($n = 4$ for HDMA and $n = 399$ for spheroids). d, e) Fluorescence images of live/dead-stained size-gradient spheroid arrays on day 7. Spheroids were treated on day 5 with different anticancer drugs at multiple concentrations for 48 h. d) Doxorubicin (DOX) and epirubicin (EPI)-treated spheroid arrays. The concentration range was 10 nM to 100 μM. e) Paclitaxel (PTX) and docetaxel (DTX)-treated spheroid arrays. The concentration range was 1 nM to 10 μM.

and compartmentalized HDMAs were introduced (**Figure** 4a). The CPMA is designed with a concave plateau and air channels to stably place the spheroid on the pillar without forming bubbles, and the dimensions are made to fit the HDMA. In addition, the outer frame of the CPMA is designed to interlock with the inner part of the HDMA chamber, allowing for easy alignment with the naked eye. In the case of compartmentalized HDMAs, partitioning walls and blocking structures were added to the bare HDMAs. The walls physically separate the liquid environment, thus allowing multiplexed conditions to be treated in a single HDMA. The blocking structures were designed to block unintended movement of spheroids.

The compartmentalization process of the spheroid array involved the use of a CPMA and a compartmentalized HDMA with

five separate reservoirs. Initially, the spheroids in the HDMA were brought into contact with the CPMA (Figure 4b). Before this step, the CPMA was coated with an anti-adherence rinsing solution by bringing it in contact with an HDMA loaded with the anti-adherence rinsing solution. Through contact, the spheroids were transferred to the CPMA, with each spheroid being separated into individual drops on the CPMA. Subsequently, the medium was loaded into the compartmentalized HDMA, and the supernatant was removed to ensure the medium remained only in each hole of the array to avoid unintended spheroid migration. The CPMA and the compartmentalized HDMA were then flipped and brought into contact. Finally, after re-flipping, the medium was carefully loaded into each reservoir for further culture in the compartmentalized HDMA. The successful transfer of spheroids to the compartmentalized HDMA using the CPMA is shown in Figure 4c. The average retention rate of spheroids at the endpoint was found to be 98.75%, indicating the high stability of the retrieval and transfer process of the spheroid array using CLiCK-Spheroid.

Next, to demonstrate the applicability of the device, we treated a single spheroid array with multiple drugs at different concentrations. Four different drugs were used: doxorubicin hydrochloride (DOX), epirubicin hydrochloride (EPI), paclitaxel (PTX), and docetaxel (DTX). Prior to drug treatment for spheroids, IC_{50} values (for 48 h) of each drug were determined for BT474 cells in two-dimensional (2D) monolayers (Figure S7, Supporting Information). By rough calculation, IC_{50} values were 1.5 μM, 1.5 μM, 4 nM, and 5.5 nM for DOX, EPI, PTX, and DTX, respectively. We observed that drugs with similar structures exhibited similar IC curves. Subsequently, we divided a size-gradient spheroid array into five horizontal compartments, applying five different concentrations of each drug for 48 h (Figure 4d,e). The results showed that damage from DOX and EPI began at concentrations of 10 μM, while PTX and DTX started causing damage at 100 nM. This indicated increased drug resistance in 3D spheroids compared to 2D cell monolayer. Finally, to perform a sequential drug treatment assay, the homogeneous spheroid array from the HDMA was transferred to a compartmentalized HDMA with five horizontal reservoirs and underwent drug treatment for 24 h (Figure S8, Supporting Information). Based on the results from the spheroid array, the treatment concentration was determined to be 10 μM, 10 μM, 100 nM, and 100 nM, for DOX, EPI, PTX, and DTX, respectively. Afterward, it was moved to another compartmentalized HDMA with five vertical reservoirs for an additional 24 h of drug treatment. Finally, the spheroid array was transferred back to the batch HDMA to stain all spheroids with live/dead reagents. This allowed the single spheroid array to be compartmentalized into 25 different groups and treated with 25 different drug combinations.

2.4. Difference in Spheroid Morphology in a Cell Composition-Gradient Spheroid Array

Similar to the generation of a size-gradient spheroid array, a cell composition-gradient spheroid array can be generated using an HDMA and a gradient block. Sequential cell seeding steps can be applied to create the composition-gradient spheroid array of two or more types of cells (Figures S1c and S9a, Supporting Information). Additionally, the configuration of the CLiCK-Spheroid needed to be different at each cell seeding step to achieve the desired composition gradient. Possible configurations include homogeneous A cell–gradient B cell, gradient A cell–reverse gradient B cell, and homogeneous A cell–gradient B cell–reverse gradient C cell. As a proof of concept, we generated a co-culture spheroid array using the composition gradient, consisting of BT474 and cytopainter green-stained BT474 (Figure S9b, Supporting Information). First, 375 000 BT474 cells were initially seeded with the gradient block-assembled HDMA, followed by the seeding of 375 000 cytopainter green-stained BT474 cells with the gradient block assembled in the opposite gradient direction. Consequently, a composition-gradient co-culture spheroid array was generated without laborious pipetting. We could observe that the actual diameter of spheroids closely matches the calculated theoretical diameter for each column (Figure S9c, Supporting Information). Meanwhile, gradual changes in GFP signals were observed depending on the column, indicating the successful formation of each gradient (Figure S9d, Supporting Information).

To analyze the effect of cell composition on spheroid morphology, we generated a composition-gradient tri-culture spheroid array composed of GFP-BT474, LF, and red fluorescent protein (RFP)-HUVECs (**Figure 5**). Initially, GFP-BT474 cells were seeded in a gradient. Following this, LF cells were seeded in a reverse gradient, and finally, RFP-HUVECs were seeded homogeneously (Figure 5a). The range of cell composition used in the experiment was determined based on the composition range employed by Nashimoto et al. to produce vascularized breast cancer spheroids (Figure 5a).[16] As a result, a composition-gradient spheroid array with a fluorescence gradient changing depending on the column was successfully generated (Figure 5b). There were initial differences between the morphology of the spheroids formed in different columns, and changes in morphology over time were also observed (Figure 5c). Even though RFP-HUVECs were seeded homogeneously, there was variation in the area of RFP expression within the spheroid array. This may be due to the promotion of HUVEC proliferation by LF, as well as the high affinity of these cell types, while BT474 cells were not well mixed with HUVECs and did not facilitate HUVEC proliferation.

To analyze the variations in the morphology of the spheroids between columns and track how their morphology changes over time, we categorized the spheroids into seven different types based on their morphology (Figure 5d) and analyzed the distribution of each type of spheroid overall, as well as the distribution by columns up to day 4 (Figure 5e,f). The distribution of morphologies can be summarized as follows: Single spheroids, consisting of LF and RFP-HUVEC, were only observed in column 1 when GFP-BT474 was absent. Stacked aggregates, characterized by indistinguishable distributions of the three cell types piled up together, predominantly appeared in regions with a higher LF ratio than BT474. This morphology was an intermediate state prevalent on day 1, which mostly disappeared from day 2. Paired spheroids were observed when a BT474 spheroid and an LF–HUVEC spheroid were adjoined side by side, with the interface where they were joined clearly visible. Due to either initial differences in ratio or changes in cell composition during growth, penetration of RFP-HUVEC and LF cells into the GFP-BT474 spheroid occurred when the proportion of BT474 increased. This phase was classified as penetrating spheroids.

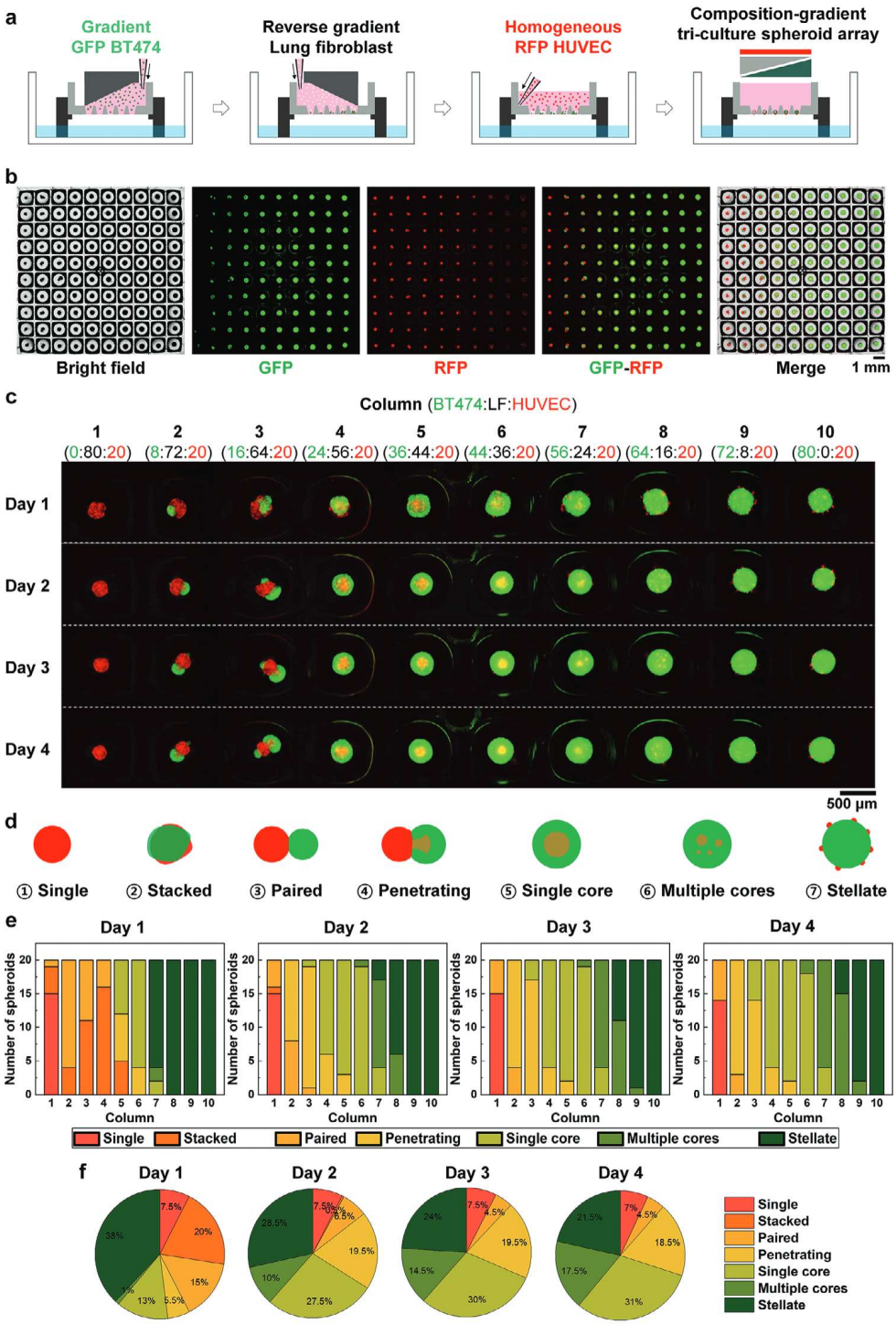

Figure 5. Spheroid analysis in a cell composition-gradient tri-culture spheroid array. a) Sequence of cell seeding to generate a composition-gradient GFP-BT474–LF–RFP-HUVEC tri-culture spheroid array. b) Microscope images of the composition-gradient spheroid array on day 4. c) Morphology changes according to the culture time. Green fluorescence indicates the breast cancer cell, while red fluorescence indicates the endothelial cell. d) Classification of tri-culture spheroids based on their morphology, including single spheroids, stacked aggregates, paired spheroids, spheroids penetrating neighboring spheroids, spheroids with a single core, spheroids with multiple cores, and stellate spheroids characterized by satellite spheroids attached to larger spheroid. e) Morphology changes of tri-culture spheroids in each column according to the culture time. f) Distribution of tri-culture spheroids by morphology over culture time.

Upon full penetration, the structure transformed into a single-core spheroid, which was distinguishable by an RFP-HUVEC–LF core surrounded by a GFP-BT474 shell. Observations suggest that when the BT474 ratio is high, it typically transitions to a single-core spheroid within a day after seeding. Between columns 7 to 10, where the BT474 ratio is substantially higher and the LF ratio is lower, multiple small LF–HUVEC or HUVEC spheroids were initially clustered around the BT474 spheroid. This arrangement resembled a star-like pattern and was classified as stellate spheroids. The stellate spheroid morphology was preserved in columns 9 to 10, where the LF proportion is extremely low. However, in columns 7 to 8, where there is a significant LF presence, the attached spheroids penetrated the BT474 spheroid over time, resulting in a multiple-core spheroid.

Interestingly, the HUVECs in the LF–HUVEC spheroid from column 2 formed vessel-like networks within the spheroid (Figure S10a, Video S3, Supporting Information). However, it was difficult to find the difference between BT474–HUVEC co-culture spheroid and BT474–LF–HUVEC tri-culture spheroid through immunostaining alone. In the case of tri-culture spheroids in the penetration process or that have become single-core spheroids, the penetrating part and the core were not visible through a confocal microscope due to the dense and opaque BT474 layers. Therefore, a spheroid-clearing process was conducted based on the method proposed by Park et al.[29] As a result, we observed a penetrating spheroid from column 2, as well as cores with a vessel network in single-core tri-culture spheroids from columns 4 and 7 (Figure S10b, Video S4, Supporting Information). These results were clearly different from BT474–HUVEC co-culture spheroids, in which HUVEC cores were not seen within the BT474 spheroid, but HUVECs were rather adhered to the surface of the BT474 spheroid. Even though the spheroids from columns 4 and 7 were both of the same single-core spheroid type, the core size was larger in spheroids from column 4, which had a higher LF ratio. Nevertheless, it was evident that the vessel network was retained regardless of the size. Lazzari et al. also reported a similar result where HUVECs were located at the core of the tri-culture spheroid with LFs and showed a network-like structure, although the cancer cell type used, pancreatic ductal carcinoma, was different.[26]

From the observations, the behavior of each cell type could be summarized as follows. BT474 cells exhibited a strong clumping force, and HUVEC alone was unable to penetrate the BT474 spheroid. This was inferred from the phenomenon where many HUVECs appeared to be attached to the outside of BT474 spheroids in the BT474–HUVEC co-culture spheroid and the rightmost columns of the composition-gradient array consisting of a low proportion of LF. On the other hand, LF could penetrate BT474, and the tendency of LF to move into the interior of the cancer cell spheroids has been reported in several studies.[16,27,28,30] When LF and HUVEC coexisted with BT474, HUVECs migrated toward LFs within the spheroid and the number of migrating HUVECs correlated with the number of seeded LFs. This can explain the reduction in the number of stellate spheroids and the increase in the number of multiple-core and single-core spheroids with decreasing column number. This was consistent with the study of Nashimoto et al. which showed a similar trend of single to multiple core spheroids depending on the ratio of MCF-7 to LF.[16] However, they did not observe stellate spheroids, presumably due to differences in the cellular affinity between MCF-7 and BT474 and the cell composition used. Furthermore, it is understood that cellular affinity can vary even among cancer cell lines from the same origin. Wan et al. reported differences in the localization of fibroblast cells within tumor spheroids of various tumor cell types.[27] They suggested that this could be due to variations in the proliferation rate of fibroblasts or differences in the expression of adhesion molecules depending on the tumor type. In this experiment, we only investigated a limited range of cell types and compositions, and while we observed corresponding differences in morphology, we could not hastily conclude which factors were involved. However, considering the effectiveness of the CLiCK-Spheroid platform in producing composition-gradient spheroid arrays by controlling cell types and numbers, as well as its flexibility in adapting seeding sequences and intervals, we believe that it will hold a favorable position for further research related to the cell composition of spheroids.

2.5. Difference in Vessel Network Formation in a Cell Composition-Gradient Spheroid Array Embedded in an Endothelial Cell-Mixed Fibrin Hydrogel

To investigate the differences in vascularization depending on the composition of tri-culture spheroids, an experiment was designed where spheroids were embedded within a fibrin hydrogel. In a previous publication, our group showed how to embed spheroid arrays within a hydrogel using a pillar array.[31,32] In this study, we embedded a composition-gradient tri-culture spheroid array within a fibrin hydrogel mixed with RFP-HUVEC to observe the interactions between the spheroids and the surrounding vessel network. Due to the compact spacing of 1.5 mm between spheroids within the HDMA, a selective CPMA with a 5 × 5 pillar array configuration was introduced to allow the collection of specific spheroid arrays, instead of retrieving the entire spheroid array (**Figure 6a**). The spacing between each pillar was set to two units. The spheroids transferred to the selective CPMA were further transferred to a low-depth well array with a 5 × 5 array format, which conformed to the dimensions of a selective CPMA. For spheroid embedding, a fibrinogen solution was loaded into each well. The spheroids were efficiently transferred to the bottom of the fibrinogen drops once in contact with the fibrinogen drop array. Subsequently, spheroids in a fibrin gel array were produced using a curing method developed in our laboratory.[33] The selected spheroid arrays were stably embedded in a fibrin gel drop array through this procedure. Since the volume of the medium drop transferred by the CPMA was small (≈0.27 μL), the fibrin gel crosslinking was not disturbed.

From the tri-culture spheroid array generated, as shown in Figure 5a, we selectively retrieved five spheroids, each from columns 2, 4, 6, 8, and 10, using a selective CPMA. These spheroids were then embedded in a 5 mg mL^{-1} fibrin hydrogel containing RFP-HUVECs at a concentration of 1 000 000 cells mL^{-1}. After 5 days of culture, we observed differences in the vessel network around the spheroids depending on the cell composition (Figure 6b–e). A higher ratio of LF within the spheroids corresponded to an increase in the area occupied by the vessel network, and a decrease in mean E lacunarity. The latter indicates

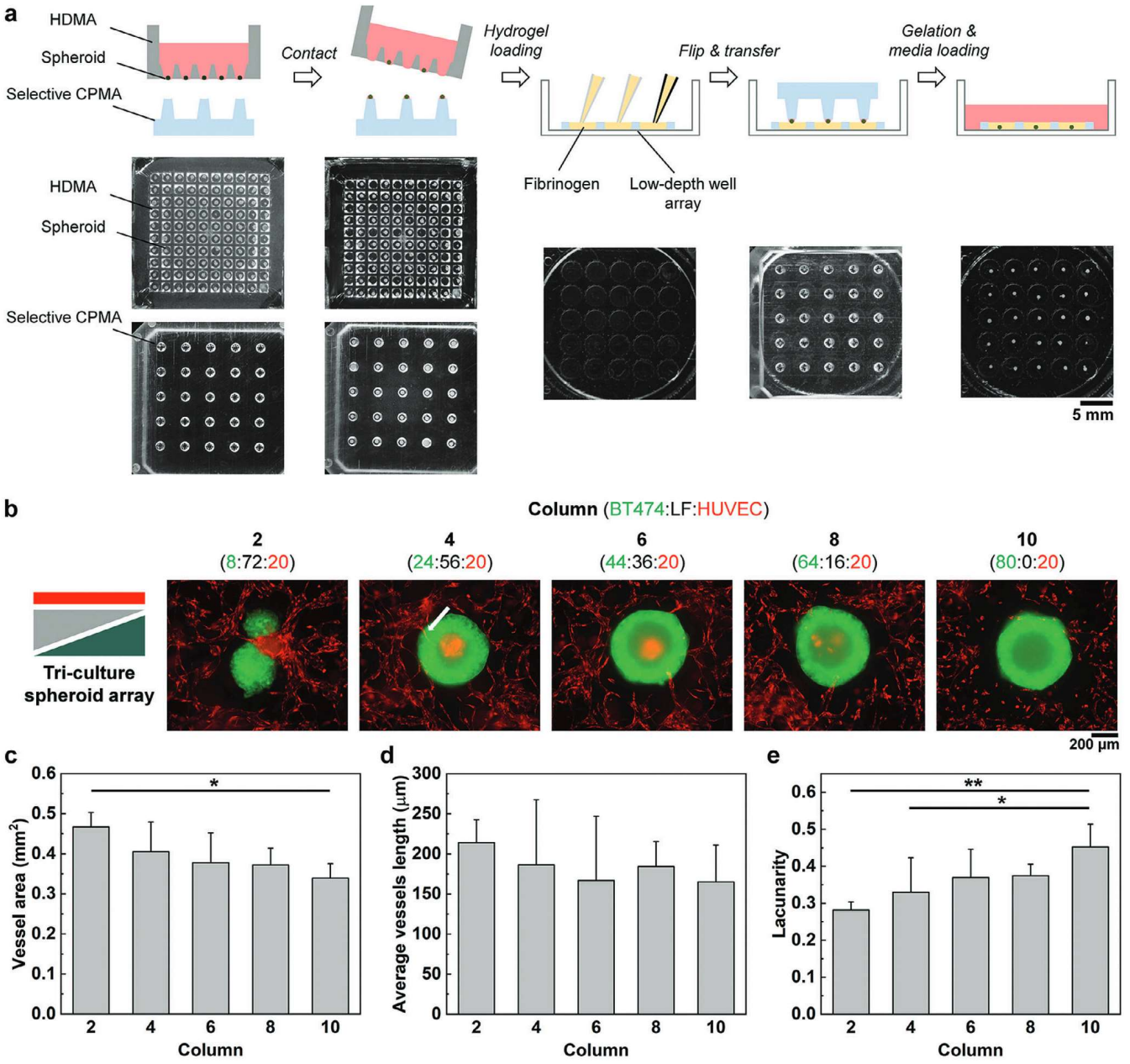

Figure 6. Embedment of a specific spheroid array using CLiCK-Spheroid. a) Schematic illustrations (top) and experimental images (bottom) of operation procedures for embedment of a specific spheroid array into a fibrin hydrogel. b) Representative spheroid images that show differences in interaction with the vessel microenvironment depending on composition. Green fluorescence indicates BT474 cells and red fluorescence indicates HUVECs. Spheroids on day 4 were transferred to the fibrin hydrogel and then cultured for 5 days. c–e) Graphs of c) the vessel area, d) the average vessel length, and e) the lacunarity of the blood vessel network in proximity to each spheroid on day 5 of fibrin embedment ($n = 5$). Significance differences were calculated by one-way analysis of variance (ANOVA) and Tukey's *post hoc* test (*$p < 0.05$, **$p < 0.01$).

a decrease in geometrical heterogeneity possibly accompanying network formation. There was no significant variation in the average vessel length. The improved formation of vessel networks with an increased proportion of LF suggests that LF aids the network formation by HUVEC, while BT474 does not engage in HUVEC growth. This observation is consistent with the findings shown in Figure 5 and previous findings that BT474 does not induce vascular sprouting.[34] When comparing the results of tri-culture spheroids in liquid with those embedded in the hydrogel, the movement of LF was different. In column 2, the LFs did not facilitate the penetration of HUVEC into the BT474 spheroids. Instead, LFs showed elongated morphology along the hydrogel. In the case of single-core spheroids from column 4, the vessel network outside the spheroid was observed to connect with the vessels within the spheroid core (Figure 6b, Figure S11, Video S5, Supporting Information). Nevertheless, the number of vessels undergoing angiogenesis toward the spheroid was quite low, possibly due to the dense spheroid formation by BT474, making

it difficult for HUVEC to penetrate through the BT474 layer. It is anticipated that using an aggressive cancer cell type or another cell line that forms less dense spheroids than BT474 could provide better observation of interaction with the vessel network.

3. Discussion

In this study, we developed a configurable and linkable in vitro 3D cell culture kit for spheroids called CLiCK-Spheroid, which can generate versatile spheroid arrays and enable on-demand retrieval and multiplexed analysis of spheroid arrays (Figure 1). To generate and retrieve spheroid arrays, we used three main components: hanging drop microarray (HDMA), gradient block, and concave pillar microarray (CPMA). We had previously reported a CPMA that was designed for separated hanging drop arrays and used for multiplexed and sequential assays.[35] However, the preparation of hanging drop arrays was labor-intensive and suffered from issues such as the height difference between drops, making consistent contact between drops challenging. The CLiCK-Spheroid overcomes these difficulties by simplifying the preparation process for hanging drop arrays and requiring fewer pipetting steps. This enhancement not only alleviates the laborious nature of the task but also eliminates the height difference between drops, which was previously problematic.

When comparing the HDMA design to multiple funnel inserts previously reported in Sumi et al.'s work,[14] the HDMA was configured to avoid placing holes directly next to the walls of the device to optimize the uniformity of the spheroids even at the expense of yield. Instead, the edges of the hole array were placed at a distance of ≈2 mm from the walls to mitigate the meniscus effect, which raises the medium height near the walls. This strategy ensured that the media height above each hole was uniform across the entire array. Our HDMA design also features vertical walls to prevent a significant increase in the size of the peripheral spheroids. Nevertheless, a slight increase in size was still observed due to the movement of cells accumulated on the bottom surface bordering the holes. To further improve homogeneity, we could potentially incorporate grooves outside the hole array of the HDMA to prevent cells accumulated on the reservoir base from entering the holes. Alternatively, we could employ a selective CPMA to harvest and utilize only the more uniformly sized spheroids, excluding the outermost spheroids of the array.

In addition to spheroid homogeneity, device utility was also increased by integrating mesh insert, gradient block, and CPMA with the HDMA. Devices in which spheroids are in one connected liquid environment, such as HDMA and microwell array, could face challenges during complete reagent change, which requires full removal of supernatant media and subsequent loading of fresh media. There was a risk that spheroids would be swept, causing them to move to adjacent holes and merge with other spheroids.[36] Moreover, during the spheroid clearing process, the addition of the dense optical clearing solution resulted in spheroid floating, which disorganized the spheroid array. However, a mesh insert effectively resolved these issues in CLiCK-Spheroid. The mesh insert, capable of reversible assembly, was introduced during the reagent change process to aid in the retention of the spheroid array and was subsequently removed to prevent interference with imaging. In the clearing process, the mesh insert also effectively prevented the spheroids from migrating to other wells. However, after adding the optical clearing solution, the mesh insert could not be detached due to the persistent buoyancy of numerous spheroids. While this obstructed bright field imaging, it did not hinder fluorescence imaging, thus proving effective for unimpeded confocal image acquisition.

The gradient blocks enable the production of spheroids in 10 different sizes in one seeding step or 10 different compositions with two to three cell seeding steps, whereas conventional methods would require the preparation of 10 different cell suspensions. The production efficiency can be further enhanced by expanding the array dimensions beyond 10 × 10. Furthermore, the gradient blocks can also be designed with various slopes, such as quadratic, cubic, or flat, to produce different types of size-gradient spheroid arrays. This flexibility allows for the customization of spheroid arrays to meet specific experimental requirements. In our experiment, we demonstrated the effect of cell composition by observing the morphology and interaction with neighbor vasculatures. Meanwhile, Cha et al.'s research categorized phenotypes based on the spatial distribution of cells and confirmed drug response trends in tri-culture spheroids using patient glioblastoma and glioblastoma cell lines.[37] Our study anticipates different outcomes if other cancer cell types were used instead of BT474, and in this context, CLiCK-Spheroid would be an appropriate platform for screening the desired morphology and composition for each cancer cell type. Additionally, Jun et al. produced hybrid spheroids composed of hepatocytes and pancreatic islet cells in varying compositions to investigate changes in liver and pancreatic characteristics compared to the mono-type liver and pancreatic islet spheroids.[38] The ability of CLiCK-Spheroid to generate composition-gradient spheroid arrays in a high-throughput manner can be applied to investigate function changes in hybrid spheroids according to cell composition, aiding in the identification of compositions of high biological relevance.

The introduction of the CPMA into the CLiCK-Spheroid platform represents a significant advancement in the retrieval and transfer of spheroid arrays. From the perspective of spheroid retrieval, CPMA can be used in CLiCK-Spheroid to maintain the position of the spheroid array while enabling retrieval of individually separated drop arrays (Figure 4a). The selective CPMA feature also facilitates the recovery of specific spheroid arrays as needed (Figure 6a). By overcoming the limitation of an inherently connected HDMA environment, this functionality broadens the utility of the CLiCK-Spheroid platform for high-throughput screening and multiplexed assays. The ability to divide or recombine a batch of spheroids as desired for reagent treatment offers several significant advantages. First, since the spheroids are grown in the same environment, they maintain synchronized conditions, which is a critical benefit for consistent experimental outcomes. Second, the flexibility to freely adjust the type of reagent and the treatment sequence for each spheroid facilitates sequential and multiplexed drug treatments. This feature enables high-throughput investigation into the effects of drug treatment sequences and drug synergies in various combinations of sequential treatments.[39,40] This approach could not be achieved with platforms in a connected liquid environment, such as traditional hanging drop microarrays or microwell arrays. Thus, CLiCK-Spheroid enhances the advantage of large-scale production of spheroids. Additionally, transferring

a spheroid array from a batch to a compartmentalized environment and vice versa is made easier, which enhances the overall throughput of spheroid array-based experiments.

Although CLiCK-Spheroid enables on-demand preparation and multiplexed analysis of diverse spheroid arrays, there are still some challenges that need to be addressed. In multiplexed condition treatment, the process of preparing serially diluted solutions and loading them into compartmentalized HDMA becomes inconvenient as the number of conditions increases. It would be more efficient to connect the platform to a microfluidic concentration gradient generator[41] to shorten the preparation process. Furthermore, there is a potential issue in compartmentalized condition treatment as spheroids within the same compartment might interfere with each other. One possible approach is to use a pillar array to treat different spheroids under multiplexed conditions without interference. To prevent the evaporation of drops, a reagent drop array containing multiple reagent types or conditions can be prepared at once using a compartmentalized HDMA and a CPMA. This array can then be applied to a spheroid array on another CPMA, allowing for individualized responses in reaction spots without interference between spheroids.

4. Conclusion

In summary, we have proposed a reconfigurable hanging drop microarray platform named CLiCK-Spheroid. This platform allows for the easy generation of highly monodispersed spheroids in the HDMA. By assembling the HDMA and gradient blocks, we can conveniently produce size-gradient and composition-gradient spheroid arrays without any cumbersome procedures. Furthermore, the spheroid arrays can be separated into individual drops or selectively retrieved using the CPMA, and transferred to compartmentalized HDMAs or hydrogel arrays. We have used this platform for multiplexed drug treatment by sequentially contacting differently compartmentalized HDMAs. Using the composition-gradient spheroid array, we have analyzed differences in morphology and vascularization based on the cell composition. The high versatility in spheroid array generation by CLiCK-Spheroid, coupled with the flexibility to separate and combine spheroid arrays on demand, is expected to enhance the convenience of spheroid array-based research, addressing the labor-intensiveness and boosting research efficiency. Potentially, our platform can also be applied to the versatile and controllable production and analysis of organoids and multi-type spheroids, providing a high-content and high-throughput in vitro screening platform to investigate drug responses and disease mechanisms with high biological relevance.

5. Experimental Section

Fabrication of CLiCK-Spheroid Components: Resin-based HDMA, CPMA molds and CPMA frames, gradient blocks, and low-depth well array molds were fabricated using DLP-type 3D printers (Pico 2 HD and Pro 4K65; Asiga, Alexandria, Australia) and a photocurable resin (SG-100; Graphy, Seoul, Korea). The printed products underwent post-processing procedures. Briefly, the products were immersed in isopropyl alcohol (IPA) and sonicated for 10 min. After drying, the products were exposed to ultraviolet (UV) light using a UV curing machine (Cure Box; ODS, Incheon, Korea), following the manufacturer's instructions. Finally, the products were autoclaved in deionized water and dried in a convection oven at 85 °C. The polycarbonate-based HDMAs, HDMA supports, and gradient blocks were produced through injection molding (Ktaewoo, Daejeon, Korea). The mesh inserts were created by attaching a surgical-grade stainless steel mesh to the printing bed of a fused deposition modeling-type 3D printer (Ender-3 V2 Neo; Creality, Shenzhen, China) and then printing polylactic acid filament on top of it.[42]

To prevent device leakage, the bottom side of HDMAs and gradient blocks were coated with hexadecyltrimethoxysilane (HDTMS). For CPMAs, the CPMA frames were first assembled with CPMA molds. Next, a mixture of poly(dimethylsiloxane) (PDMS) (monomer: curing agent = 10:1) was poured into the molds and degassed in a vacuum chamber. After degassing, they were cured in a convection oven at 85 °C. To fabricate low-depth well arrays, a small amount of PDMS was poured on low-depth well array molds. Then, inverted confocal dishes were placed on top of the molds to minimize the entrapment of bubbles within the mold. Next, the entire assembly was inverted, and magnets were placed on the top of the mold and the bottom of the confocal dish to prevent separation between them. Afterward, the same process as CPMA fabrication was followed. To prevent contamination, HDMAs and gradient blocks were autoclaved and dried before use. The mesh inserts and low-depth well arrays were immersed in filtered 100% ethanol and dried while being exposed to UV overnight in a clean bench.

Cell Culture: A human breast cancer cell line BT474 (Korean Cell Line Bank, Seoul, Korea) and a GFP expressing BT474 (BT474/GFP stable cell line; FenicsBio, Halethorpe, MD, USA) were cultured in Dulbecco's Modified Eagle Medium (DMEM) with 10% fetal bovine serum and 1% penicillin-streptomycin. Normal human LF (Lonza, Basel, Switzerland) and RFP expressing LFs (RFP-HLFCs-ad; Angio-Proteomie, Boston, MA, USA) were cultured in a fibroblast growth medium-2 (FGM-2, Lonza), and cells under passage 7 were used. HUVECs (Lonza) and RFP expressing HUVECs (RFP-HUVECs; Angio-Proteomie) were cultured in an endothelial growth medium-2 (EGM-2, Lonza), and cells under passage 5 were used. The medium in the cell culture dishes was replaced every 2 days.

To produce spheroids using commercial devices, a cell suspension was prepared at the desired concentration. The cell suspension was then seeded into a 96-well spheroid microplate (#4515; Corning, NY, USA) and a conventional microwell array device (StemFIT 1000; MicroFIT, Hanam, Korea) according to the manufacturer's instructions.

Preparation of Fibrin Hydrogel: A fibrinogen solution was prepared by mixing fibrinogen obtained from bovine plasma (Sigma-Aldrich, St. Louis, MO, USA) with PBS (Corning) to achieve a final fibrinogen concentration of 2.5 mg mL^{-1}. The prepared fibrinogen solution was filtered using a 0.22 µm syringe filter for sterilization. Thrombin solution was prepared at two concentrations: 50and 5 U mL^{-1} for the preparation of fibrin hydrogel. The 50 U mL^{-1} fibrin solution was loaded into a mist sprayer for temporary fibrin crosslinking, while complete crosslinking was achieved by immersing the temporarily crosslinked hydrogel in the 5 U mL^{-1} fibrin solution.[33]

Live/Dead Assay of Spheroids: To investigate the spheroid viability and necrotic core formation, this work performed live/dead staining. Spheroids were stained with 4 µM calcein-AM (Invitrogen, Carlsbad, CA, USA) and 10 µM propidium iodide (P1304MP; Thermo Fisher, Waltham, MA, USA) for 30 min at 37 °C. After the staining, the medium was replaced with a fresh culture medium. The spheroids were imaged with a fluorescence microscope (F1-CIS; Nanoscope Systems, Daejeon, Korea).

Drug Treatment to 2D Monolayer Cells: To determine IC_{50} values of anticancer drugs for 48 h, BT474 cells seeded on the 96-well plates were used. The cells were seeded in a concentration of 10 000 cells $well^{-1}$ and were cultured for 4 days. Next, 200 µL of serially diluted drug solutions, including doxorubicin, epirubicin, paclitaxel, and docetaxel, were loaded into each well and cultured for an additional 48 h. Following the drug treatment, Cell Counting Kit-8 (CCK-8; Dojindo, Kumamoto, Japan) was used to measure the drug response. Briefly, the CCK-8 stock solution was diluted by mixing it with the appropriate cell culture medium at a ratio of 1:10, and the target cells were treated with the solution for 4 h. Then, 50 µL of the solution was retrieved and mixed with 50 µL PBS, and the absorbance was measured with a microplate spectrophotometer (Spectra-

Max 250; Molecular Devices, Sunnyvale, CA, USA) set at a wavelength of 450 nm.

Western Blotting: A Western blot was performed on spheroids following a similar method to a previous study.[43] The spheroids were lysed in RIPA buffer (GenDEPOT, Katy, TX, USA) by homogenizing them with an ultrasonic processor (VCX-750; Sonics & Materials, Newtown, CT, USA). The concentration of each protein lysate was measured by using Pierce BCA Protein Assay Kit (Thermo Fisher) and equalized at a concentration of 1 μg μL^{-1}. The lysates were denatured by boiling at 95 °C with the addition of 5X SDS-PAGE Loading Buffer (LPS solution, Daejeon, Korea). 10 μL protein samples were run on 10% sodium dodecyl sulfate (SDS)-polyacrylamide gel and transferred to a nitrocellulose membrane (Merck). The membranes were blocked with a 3% bovine serum albumin (BSA) solution at room temperature (RT) for 1 h and incubated in the blocking solution containing respective primary antibodies overnight at 4 °C. The primary antibodies used were Cyclin D1 (sc-20044; 1:500, Santa Cruz Biotechnology, Dallas, TX, USA), c-Myc (sc-40; 1:1000, Santa Cruz Biotechnology), HER2/ErbB2 (#2165; 1:1000, Cell Signaling Technologies), ERα (#15 580; 1:1000, Invitrogen), p-AKT Ser473 (#4051; 1:1000, Cell Signaling Technologies), AKT (#9272; 1:1000, Cell Signaling Technologies), ERK1/2 (#9102; 1:1000, Cell Signaling Technologies), p-ERK1/2 (#9101; 1:1000, Cell Signaling Technologies). The membranes were then incubated with horseradish peroxidase (HRP)-conjugated anti-mouse antibody (#7076; 1:1000, Cell Signaling Technologies, Danvers, MA, USA), anti-rabbit antibody (#7074; 1:1000, Cell Signaling Technologies), and glyceraldehyde 3-phosphate dehydrogenase (GAPDH)-HRP (sc-47724 HRP; 1:1000, Santa Cruz Biotechnology) for 1 h at RT. Bands of each protein were detected on the iBright CL750 Imaging System (Thermo Fisher), and their intensity was analyzed using the ImageJ software.

Spheroid Immunostaining and Clearing: The spheroids were immunostained and cleared based on a previous study to observe the internal structure of tri-culture spheroids.[29] Briefly, spheroids were first fixed in a 4% formaldehyde solution for 20 min, followed by 1 h permeabilization in a 0.1% triton-X solution and 30 min blocking with 5% BSA. After delipidation with SDS-based clearing buffer (300 mM SDS, 10 mM sodium borate, 100 mM sodium sulfite, pH 9.0) for 6 h, appropriate markers were stained with antibodies, followed by 1 h post-fixation. The optical clearing was performed using a Protos-based immersion medium (125 g iohexol, 3 g diatrizoic acid, 5 g N-methyl-D-glucamine dissolved in 100 mL distilled water with the refractive index adjusted to 1.458 by adding DI water) until the spheroids became transparent. The cleared spheroids were imaged with a fluorescence microscope (F1-CIS) for array image acquisition or a confocal microscope (LSM 980; Carl Zeiss, Oberkochen, Germany) at the KAIST Analysis Center for Research Advancement (KARA).

Analysis of Vascular Network Formation: The vascular network formed by HUVECs in fibrin hydrogel was analyzed with AngioTool (version 0.6a).[42,44]

Statistical Analysis: The mean ± standard deviation was used to express the data. A one-way analysis of variance (ANOVA) with a Tukey *post-hoc* test was performed in IBM SPSS Statistics 26 to compare the data from five groups in spheroid arrays with a vascular network. For comparing the data from two groups, the two-tailed student *t*-test was used. *p* values >0.05, <0.05, and <0.01 were considered to be not significant (n.s.), statistically significant (*), and very significant (**), respectively.

Supporting Information

Supporting Information is available from the Wiley Online Library or from the author.

Acknowledgements

This work was supported by the National Research Foundation of Korea (NRF) funded by the Korean government (MSIT) (NRF-2022R1A2B5B03002198).

Conflict of Interest

The authors declare no conflict of interest.

Data availability Statement

The data that support the findings of this study are available from the corresponding author upon reasonable request.

Keywords

contact-based spheroid transfer, gradient spheroid array, hanging drop, spheroids, tumor microenvironment

Received: February 8, 2024
Revised: May 25, 2024
Published online: June 8, 2024

[1] A. Abbott, *Nature* **2005**, *438*, 144.
[2] J. Zurlo, D. Rodacille, A. M. Goldberg, *Environ. Health Perspect.* **1996**, *104*, 878.
[3] H. R. Ferdowsian, N. Beck, *PLoS One* **2011**, *6*, e24059.
[4] T. Takebe, K. Sekine, M. Enomura, H. Koike, M. Kimura, T. Ogaeri, R. R. Zhang, Y. Ueno, Y. W. Zheng, N. Koike, S. Aoyama, Y. Adachi, H. Taniguchi, *Nature* **2013**, *499*, 481.
[5] F. Soldner, R. Jaenisch, *Science* **2012**, *338*, 1155.
[6] M. Kim, H. Mun, C. O. Sung, E. J. Cho, H. J. Jeon, S. M. Chun, D. J. Jung, T. H. Shin, G. S. Jeong, D. K. Kim, E. K. Choi, S. Y. Jeong, A. M. Taylor, S. Jain, M. Meyerson, S. J. Jang, *Nat. Commun.* **2019**, *10*, 3991.
[7] A. R. Mazzocchi, S. A. P. Rajan, K. I. Votanopoulos, A. R. Hall, A. Skardal, *Sci. Rep.* **2018**, *8*, 2886.
[8] G. Fang, Y. C. Chen, H. Lu, D. Jin, *Adv. Funct. Mater.* **2023**, *33*, 2215043.
[9] S. M. Kang, D. Kim, J. H. Lee, S. Takayama, J. Y. Park, *Adv. Healthcare Mater.* **2021**, *10*, 2001284.
[10] R. Rasouli, M. Tabrizian, *Small* **2021**, *17*, 2101931.
[11] S. Sart, R. F.-X. Tomasi, G. Amselem, C. N. Baroud, *Nat. Commun.* **2017**, *8*, 469.
[12] S. W. Lee, S. Y. Jeong, T. H. Shin, J. Min, D. Lee, G. S. Jeong, *PLoS One* **2019**, *14*, e0219834.
[13] G. H. Lee, J. S. Lee, G. H. Lee, W. Y. Joung, S. H. Kim, S. H. Lee, J. Y. Park, D. H. Kim, *Biofabrication* **2018**, *10*, 015001.
[14] S. Sumi, M. Kawagoe, R. Abe, G. Yanai, K. C. Yang, Y. Shirouzu, *Regen. Ther.* **2017**, *7*, 52.
[15] G. Fang, H. Lu, A. Law, D. Gallego-Ortega, D. Jin, G. Lin, *Lab Chip* **2019**, *19*, 4093.
[16] Y. Nashimoto, R. Okada, S. Hanada, Y. Arima, K. Nishiyama, T. Miura, R. Yokokawa, *Biomaterials* **2020**, *229*, 119547.
[17] S. Däster, N. Amatruda, D. Calabrese, R. Ivanek, E. Turrini, R. A. Droeser, P. Zajac, C. Fimognari, G. C. Spagnoli, G. Iezzi, V. Mele, M. G. Muraro, *OncoTargets Ther.* **2017**, *8*, 1725.
[18] L. Deng, Z. Feng, H. Deng, Y. Jiang, K. Song, Y. Shi, S. Liu, J. Zhang, S. Bai, Z. Qin, A. Dong, *ACS Appl. Mater. Interfaces* **2019**, *11*, 31743.
[19] A. Yamamoto, Y. Huang, B. A. Krajina, M. McBirney, A. E. Doak, S. Qu, C. L. Wang, M. C. Haffner, K. J. Cheung, *Proc. Natl. Acad. Sci. USA* **2023**, *120*, e2214888120.
[20] A. Mazzocchi, S. Soker, A. Skardal, in *Tumor Organoids*, (Eds: S. Soker, A. Skardal), Humana Press, Totowa, NJ **2018**.
[21] M. Marimuthu, N. Rousset, A. St-Georges-Robillard, M. A. Lateef, M. Ferland, A. M. Mes-Masson, T. Gervais, *Lab Chip* **2018**, *18*, 304.
[22] A. Ganguli, A. Mostafa, C. Saavedra, Y. Kim, P. Le, V. Faramarzi, R. W. Feathers, J. Berger, K. P. Ramos-Cruz, O. Adeniba, G. J. P. Diaz,

J. Drnevich, C. L. Wright, A. G. Hernandez, W. Lin, A. M. Smith, F. Kosari, G. Vasmatzis, P. Z. Anastasiadis, R. Bashir, *Sci. Adv.* **2021**, *7*, eabc1323.
[23] W. Liu, M. Sun, B. Lu, M. Yan, K. Han, J. Wang, *Sens. Actuators, B Chem.* **2019**, *292*, 111.
[24] C. Eilenberger, M. Rothbauer, F. Selinger, A. Gerhartl, C. Jordan, M. Harasek, B. Schädl, J. Grillari, J. Weghuber, W. Neuhaus, S. Küpcü, P. Ertl, *Adv. Sci.* **2021**, *8*, 2004856.
[25] F. Hirschhaeuser, H. Menne, C. Dittfeld, J. West, W. Mueller-Klieser, L. A. Kunz-Schughart, *J. Biotechnol.* **2010**, *148*, 3.
[26] G. Lazzari, V. Nicolas, M. Matsusaki, M. Akashi, P. Couvreur, S. Mura, *Acta Biomater.* **2018**, *78*, 296.
[27] Z. Wan, M. A. Floryan, M. F. Coughlin, S. Zhang, A. X. Zhong, S. E. Shelton, X. Wang, C. Xu, D. A. Barbie, R. D. Kamm, *Adv. Healthcare Mater.* **2023**, *12*, 2201784.
[28] I. Yakavets, A. Francois, A. Benoit, J. L. Merlin, L. Bezdetnaya, G. Vogin, *Sci. Rep.* **2020**, *10*, 21273.
[29] Y. G. Park, C. H. Sohn, R. Chen, M. McCue, D. H. Yun, G. T. Drummond, T. Ku, N. B. Evans, H. C. Oak, W. Trieu, H. Choi, X. Jin, V. Lilascharoen, J. Wang, M. C. Truttmann, H. W. Qi, H. L. Ploegh, T. R. Golub, S. C. Chen, M. P. Frosch, H. J. Kulik, B. K. Lim, K. Chung, *Nat. Biotechnol.* **2019**, *37*, 73.
[30] J. Park, S. Kim, J. Hong, J. S. Jeon, *Lab Chip* **2022**, *22*, 4335.
[31] H. Roh, H. Kim, J. K. Park, *Biosensors* **2021**, *11*, 506.
[32] H. Kim, C. H. Cho, J. K. Park, *Biomicrofluidics* **2018**, *12*, 044109.
[33] S. J. Kim, G. Lee, J. K. Park, *Adv. Mater. Technol.* **2022**, *7*, 2101326.
[34] M. Gadde, C. Phillips, N. Ghousifam, A. G. Sorace, E. Wong, S. Krishnamurthy, A. Syed, O. Rahal, T. E. Yankeelov, W. A. Woodward, M. N. Rylander, *Biotechnol. Bioeng.* **2020**, *117*, 3572.
[35] H. Kim, H. Roh, H. Kim, J. K. Park, *Lab Chip* **2021**, *21*, 4155.
[36] E. O. Mosaad, K. F. Chambers, K. Futrega, J. A. Clements, M. R. Doran, *Sci. Rep.* **2018**, *8*, 253.
[37] J. Cha, W. Sim, I. Yong, J. Park, J. K. Shim, J. H. Chang, S. G. Kang, P. Kim, *Cancers (Basel)* **2022**, *14*, 5910.
[38] Y. Jun, A. R. Kang, J. S. Lee, G. S. Jeong, J. Ju, D. Y. Lee, S. H. Lee, *Biomaterials* **2013**, *34*, 3784.
[39] R. Zhang, J. Yang, M. Sima, Y. Zhou, J. Kopeček, *Proc. Natl. Acad. Sci. USA* **2014**, *111*, 12181.
[40] B. Schuster, M. Junkin, S. S. Kashaf, I. Romero-Calvo, K. Kirby, J. Matthews, C. R. Weber, A. Rzhetsky, K. P. White, S. Tay, *Nat. Commun.* **2020**, *11*, 5271.
[41] J. Park, H. Roh, J. K. Park, *Micromachines* **2019**, *10*, 174.
[42] S. J. Kim, G. Lee, J. K. Park, *ACS Appl. Mater. Interfaces* **2023**, *15*, 41247.
[43] B. Kim, Y. Koh, H. Do, Y. Ju, J. Bin Choi, G. Cho, H. W. Yoo, B. H. Lee, J. Han, J. E. Park, Y. M. Han, *Int. J. Mol. Sci.* **2022**, *23*, 13861.
[44] E. Zudaire, L. Gambardella, C. Kurcz, S. Vermeren, *PLoS One* **2011**, *6*, e27385.